Published in final edited form as:
J Magn Reson Imaging. 2008 May ; 27(5): . doi:10.1002/jmri.21326.

Adaptations in Trabecular Bone Microarchitecture in Olympic Athletes Determined by 7T MRI

Gregory Chang, MD[1,*], **S. Kubilay Pakin, PhD**[2], **Mark E. Schweitzer, MD**[1], **Punam K. Saha, PhD**[3,4], and **Ravinder R. Regatte, PhD**[1]

[1]Center for Biomedical Imaging, Department of Radiology, NYU School of Medicine, Hospital for Joint Disease, New York, New York, USA

[2]VirtualScopics, Inc., Rochester, New York, USA

[3]Department of Electrical and Computer Engineering, University of Iowa, Iowa City, Iowa, USA

[4]Department of Radiology, University of Iowa, Iowa City, Iowa, USA

Abstract

Purpose—To produce in vivo high-resolution images of the knee and to determine the feasibility of using 7T MR to detect changes in trabecular bone microarchitecture in elite athletes (Olympic fencers) who undergo high impact activity.

Materials and Methods—The dominant knees of four males from the U.S. Olympic Fencing Team and three matched healthy male controls were scanned in a 7T whole-body scanner using a quadrature knee coil with three-dimensional (3D) fast low angle shot (FLASH): 50 axial images at the distal femur (0.156 mm × 0.156 mm) and 80 axial images at the knee joint (0.195 mm × 0.195 mm). Bone volume fraction (BVF) and marrow volume fraction (MVF) images were computed and fuzzy distance transform (FDT) and digital topological analysis (DTA) were applied to determine: trabecular number (Tb.N), trabecular thickness (Tb.Th), and trabecular separation (Tb.Sp); BVF (BV/TV); trabecular and marrow space surface-to-curve ratio (SC, marker of plate to rod ratio); and trabecular and marrow space erosion index (EI, inverse marker for network connectivity). Quadriceps muscle volume (MV) was calculated as well. We calculated group means and performed two-tailed *t*-tests to determine statistical significance.

Results—Compared to controls, fencers had: decreased Tb.Sp ($P = 0.0082$ at femur, $P = 0.051$ at joint); increased Tb.N ($P < 0.05$ at both femur and joint) and BV/TV ($P < 0.001$ at both femur and joint); increased trabecular SC and decreased marrow space SC ($P < 0.01$ at both femur and joint); decreased trabecular EI and increased marrow space EI ($P < 0.01$ at both femur and joint); and increased MV ($P = 0.038$). There was no difference in Tb.Th at the distal femur ($P = 0.92$) or joint ($P = 0.71$) between groups.

Conclusion—To our knowledge, this is the first study to perform 7T MRI of the knee in vivo. Elite athletes who undergo high impact activity have increased MV and improved trabecular bone structure compared to controls.

Keywords

fuzzy distance transform; digital topology; trabecular bone; Olympic fencers; fracture risk; osteoporosis; osteoarthritis

[*]Address reprint requests to: G.C., MD, Center for Biomedical Imaging, Department of Radiology, NYU School of Medicine, Hospital for Joint Disease, 301 East 17th Street. New York, NY 10003. changg02@med.nyu.edu.

The National Institutes of Health (NIH) consensus panel on osteoporosis defined it as a "skeletal disorder characterized by compromised bone strength predisposing a person to an increased risk of fracture" (1). Though bone mineral density (BMD), as assessed by dual energy X-ray absorptiometry (DEXA), is the parameter currently used to diagnose osteoporosis and assess fracture risk, many studies have concluded that trabecular bone microarchitecture is as important as BMD in determining bone strength and fracture risk (2–5).

In recent years, high-resolution micro-MRI (~100–200 μm) has become a promising noninvasive technique to evaluate and produce images of trabecular bone structure (6,7). Furthermore, the development of novel postprocessing techniques, such as fuzzy distance transform (FDT) (8,9) and digital topological analysis (DTA) (10–12), has provided researchers with the means to quantitatively assess trabecular bone morphology and topology.

Until now, most of these studies have been performed at 1.5T, which can be limited by long scan times and low signal-to-noise ratio (SNR). In recent years, there has been increasing interest in imaging at higher field strengths for musculoskeletal applications (13–15). Scanning at higher field strengths has the potential to provide improved SNR and spatial resolution and to decrease the amount of time required for scanning (16). Disadvantages of scanning at higher field strengths also exist, such as stronger magnetic susceptibility and larger chemical shift artifacts. For example, the chemical shift difference between water and fat resonance at 7T is ~1040 Hz compared to ~440 Hz at 3T and ~220 Hz at 1.5T (16). At a bandwidth of 130 Hz (used in this study), this corresponds to a chemical shift of eight pixels at 7T, vs. 3.4 pixels at 3T and 1.7 pixels at 1.5T. Furthermore, changes in relaxation time (increase in T_1 and decrease in T_2 as the static field strength increases) may lead to decreased contrast resolution. Thus, pulse sequence parameters have to be reoptimized if they are to be utilized at higher field strength.

The goals of our current study were the following: 1) to utilize a whole-body 7T MRI system to produce high-resolution in vivo images of trabecular bone at the knee; and 2) to determine the feasibility of using 7T MRI to detect differences in trabecular bone microarchitecture among subjects by analyzing the images with FDT and DTA. For our subjects, we chose to compare a small group of elite athletes, members of the 2004 U.S. Olympic Fencing Team, and a group of age- and weight-matched controls who maintained normal levels of physical activity. The members of the Olympic fencing team are unique in that they have subjected their lower extremities to intense mechanical loading over several years. Wolff's Law states that bone is deposited in accordance with the mechanical forces placed upon it (17). We therefore hypothesized that trabecular bone quality in these elite athletes would demonstrate improvements in structural parameters that allow it to withstand elevated mechanical loads, and we hypothesized that these features would be detectable by 7T MRI.

MATERIALS AND METHODS

Human Subjects

This study was approved by the Institutional Review Board at our institution (New York University School of Medicine). We recruited four male members of the 2004 U.S. Olympic Fencing Team who were actively training four to eight hours per day, six days per week, and three healthy male controls matched for age, height, and weight, who exercised no more than three times per week. The average age, height, and weight for the fencers was 26 years, 1.81 m, and 81.8 kg, respectively, vs. 25 years, 1.82 m, and 77.3 kg, respectively, for the

controls. All participants in the study were volunteers, and written informed consent was obtained from all subjects. All subjects were screened for contraindications to undergoing an MRI examination. Both bone data as well as muscle volume data were obtained to provide an internal control for bone mechanical stress.

MR Scanning

The knee of the leading lower extremity of each subject (from a distance approximately 90% along the length of the femoral shaft to a point approximately 10% along the length of the tibial shaft) was scanned on a 7T whole-body MR scanner (Siemens Medical Solutions, Erlangen, Germany) using a quadrature knee coil (18-cm diameter, transmit-receive). A high-resolution three-dimensional fast low angle shot (3D-FLASH) sequence was employed to obtain all images (TR/TE = 20 msec/4.5 msec; flip angle = 10°; bandwidth = 130 Hz/pixel; one signal acquired; 80 axial images at the level of the knee joint with resolution 0.195mm × 0.195 mm × 1 mm and 50 axial images at the level of the distal femur with resolution 0.156 mm × 0.156 mm × 1 mm. Scanning time was ~12 minutes total.

Image Processing: Apparent Bone Volume Fraction and Marrow Volume Fraction Maps

All images were anonymized before image processing and analysis. To process the images, a region of interest (ROI) of trabecular bone was selected on each image by drawing a boundary approximately 1 mm from the endosteal surface of cortical bone. Bone volume fraction (BVF) images were then computed using a local marrow intensity computation approach without requiring a global thresholding. In a BVF image, pixel intensity corresponds to the fractional occupancy of bone. Marrow volume fraction (MVF) images were also created by taking the inverse of BVF images. Next, subvoxel processing was applied, in which voxels were subdivided and signal intensities were redistributed among the subvoxels. This produces images with apparent higher spatial resolution. For FDT, these BVF maps were used directly. For DTA, an additional step was performed in which the BVF maps were skeletonized, creating a surface representation consisting of 1D and 2D structures (curves and surfaces, respectively).

FDT and Quantitative Assessment of Trabecular Bone Thickness and Separation

At the in vivo spatial resolution of MR images of trabecular bone, the borders of individual trabeculae are indistinct secondary to partial volume effects and noise. FDT is a method that allows accurate distance measurements in the presence of partial volume effects using grayscale MR images (9). In a grayscale image of a fuzzy object, the length of a path is computed as an integral of gray values along the path and then the distance between two given points is evaluated by considering all the paths between these two points. FDT at a pixel is computed as the fuzzy distance between the pixel and the background (regions with zero intensity). Finally, the thickness of a structure is computed by sampling FDT values along the skeleton of the target structure and then estimating the average. BVF images are used for computing trabecular thickness while MVF images are used for trabecular separation.

DTA Image and Quantitative Assessment of Topology

DTA (10) is a fully 3D method that accurately determines the topological class (e.g., surfaces, curves, junctions, and edges) of each individual location in a digitized structure that has been applied for quantifying quality of trabecular bone architectural makeup (11). Before applying DTA, a binarized trabecular bone image is skeletonized to a network of 1D and 2D structures representing rods and plates, respectively. DTA involves three steps; the first one is inspecting each bone voxel's 26 neighborhood (i.e., the 26 other voxels within the voxel's 3 × 3 × 3 kernel) and computation of the numbers of objects, tunnels, and

cavities under a hypothetical conversion of the central voxel to marrow. A partial classification of each bone voxel is determined from these three numbers using a lookup table for an idealized network of surfaces and curves. A unique topological classification is then achieved using the results of partial classification and another lookup table solving for local topological ambiguities in digital manifolds and their junctions (10,11). These topological classes are used to compute several topological parameters for trabecular bone (TB) networks. We focused on two specific parameters; namely, the surface-to-curve ratio (SC) and the erosion index (EI). The SC represents the trabecular plate to rod ratio, which has clinical importance, being known to decrease in subjects with osteoporosis (18,19). The EI is a surrogate of network connectivity, and represents the ratio of parameters expected to increase during osteoclastic resorption (curve, curve-edge, surface-edge, profile-edge, and curve-curve junctions) relative to those expected to decrease (surface and surface-surface). A higher EI indicates a decrease in network connectivity. In subjects with osteoporosis, connectivity between rods has been shown to decrease (20).

Measurement of Muscle Volume

For each axial image, an ROI was manually drawn on each quadriceps muscle. Muscle volume was calculated as cross-sectional muscle area multiplied by slice thickness (1 mm) and number of slices.

Data Analysis and Statistical Analysis

Volumes of interest at the distal femur and at the level of the knee joint were selected (Fig. 1). For each group, means and standard deviations (SDs) were calculated for muscle volumes, trabecular bone morphologic parameters (trabecular thickness, trabecular separation, trabecular number, and trabecular fraction), and trabecular bone topologic parameters (SC, EI) within each volume of interest. Marrow space topologic parameters (SC, EI) for each volume of interest were also calculated. Two-tailed Student's *t*-tests were performed using Microsoft Excel 2003, with $P < 0.05$ considered to indicate a significant difference.

RESULTS

Representative axial images of the distal femur and proximal tibia with ROIs are shown (Fig. 2a and b).

At both the distal femur and the level of the knee joint, there was no difference in trabecular thickness in the fencers compared to the controls (Tables 1 and 2). However, at both the distal femur and at the knee joint, the fencers demonstrated increased trabecular number, increased BVF fraction, and decreased trabecular separation compared to the controls ($P < 0.05$ for all, Tables 1 and 2).

With regard to the topology of the trabeculae, the fencers had increased trabecular plate-like structure (increased SC) and increased trabecular network connectivity (decreased EI) at both the distal femur and at the level of the joint compared to the controls ($P < 0.01$) (Table 3). Similarly, the fencers had decreased plate-like marrow structure and decreased marrow network connectivity (increased EI) at both the distal femur and at the level of the joint compared to controls ($P < 0.01$) (Table 4). Quadriceps muscle volumes were also greater in the fencers compared to the controls ($P < 0.05$) (Table 5).

DISCUSSION

To our best knowledge, this is the first study to perform in vivo high-resolution MRI of trabecular bone at 7T. This study also demonstrates the feasibility of using 7T MR to quantitatively assess and detect differences in trabecular bone microarchitecture among subjects. While prior studies at lower field strength have elucidated how trabecular bone microarchitecture changes in osteoporosis (2,3,5), osteoporosis after treatment (21,22), and osteoarthritis (23,24), we have investigated how trabecular bone microarchitecture adapts in response to intense mechanical loading, such as that endured by the lower extremities of world-class athletes. Specifically, the results show that Olympic fencers have apparent changes in both morphologic and topologic parameters of trabecular bone microarchitecture compared to matched controls.

High-resolution MRI of trabecular bone ideally produces accurate representations of individual trabeculae and marrow spaces with regard to size, shape, orientation, and connectivity. The advantage of performing MRI of trabecular bone at high field strength is the greater SNR, which allows the flexibility for decreased scan time and/or increased spatial resolution. Our initial goal was to determine the feasibility of performing in vivo high-resolution MRI of trabecular bone of the knee at 7T. Critical to the performance of this task was the utilization of a dedicated quadrature knee coil. While many sequences are in use for MRI of trabecular bone at 1.5T and 3T (7), we decided to utilize a 3D-FLASH sequence, which has the advantage of a short repetition time. We aimed to decrease scan time rather than increase the spatial resolution observed in prior studies (Table 6). The greater SNR at 7T allowed the scan time to be reduced to ~12 minutes to obtain 130 axial images (greater than 10 images per minute), as opposed to up to 20 minutes when scanning at lower field strengths (two to eight images per minute) (Table 6). Such reduction in scan time decreases the chance for motion artifact, which is detrimental to micro-MR imaging even if it is submillimeter in scale.

It was not possible to scan our subjects at lower field strength and make a direct comparison of SNR, but the improvement in SNR at 7T can be estimated. Theoretically, the signal intensity from a MR experiment is proportional to the square of the static magnetic field (B_0^2). Noise is due to a combination of radiofrequency (RF) coil noise and sample noise. If all noise were to come from the RF coil, noise would be directly proportional to one-quarter of the static field ($B_0^{1/4}$), resulting in an SNR that is proportional to $B_0^{7/4}$ (25). At higher field strengths, sample noise becomes a more important contributor, and in this scenario, noise is proportional to B_0, which would result in a SNR proportional to B_0. Therefore, ideally the SNR can be expected to increase at least 4.6 (7/1.5) times at 7T compared to 1.5T (2.3 times compared to 3T).

In order to perform quantitative assessment of trabecular bone microarchitecture at higher field strength, the most important technical obstacle to be surmounted is the increased susceptibility artifact, which can lead to artifactual broadening of the trabecular bone signal void. For example, in a recent study of calcaneal bone structure, 3T results were found to overestimate trabecular thickness (0.220 ± 0.020 mm vs. 0.180 ± 0.020 mm) and bone fraction (0.41 ± 0.04 vs. 0.28 ± 0.04) by approximately 25% to 30% when compared to 1.5T results (15). Since susceptibility increases with the square of B_0, one would expect 7T results to overestimate trabecular thickness and BVF to an even greater extent than at 3T. In the worst case scenario, such overestimation would obscure measurable differences in trabecular bone microarchitecture between subjects and make it infeasible to perform quantitative assessment. We discovered, however, that trabecular thickness in the current study (0.220 ± 0.005 mm) is similar to that observed in the recent 3T study of the calcaneus (0.220 ± 0.020 mm) (15) and a recent 1.5T study of the knee (0.222 ± 0.006 mm) (24). In

addition, the BVF in our study (0.287 ± 0.006) is similar to that reported in 1.5T data from the calcaneus (0.28 ± 0.04) (15) and 1.5T data from the knee (0.29 ± 0.012) (24). Comparison with previously published studies does not validate our measurements, but the similarities in values raises promise for the 7T technique. The reason why trabecular thickness and BVF are not overestimated to an even greater extent at 7T may be the greater SNR at 7T and the slightly shorter TE we have utilized. Together, these could decrease the amount of susceptibility artifact on images. The results suggest that despite increased susceptibility artifact and intravoxel phase dispersion at 7T (which should lead to overestimation of trabecular thickness and BVF), quantitative assessment of trabecular bone microarchitecture is feasible and can be performed with a decreased scan time.

The sport of fencing involves short bursts of high impact activity, such as when the athletes are lunging or rapidly changing directions. Wolff's Law states that bone is deposited in accordance with the mechanical forces placed upon it, and many studies have demonstrated that high-impact physical activity results in elevated BMD as measured by DEXA or quantitative computed tomography (qCT) (26–29). This study suggests that trabecular bone microarchitecture might adapt as well. Specifically, compared to matched controls, the lower extremities of Olympic fencers demonstrate apparent improvements in both morphologic (increased trabecular number, increased BVF, and decreased trabecular separation) and topologic parameters (increased plate-like structure and network connectivity) of trabecular bone microarchitecture (with the corresponding opposite changes in marrow space topology). The fencers have increased muscle volumes as well. Presumably, the increased muscle volumes result in greater mechanical forces being directly transmitted to bone, which could contribute to bone remodeling.

The apparent trabecular bone microarchitectural adaptations in the Olympic fencers are the converse of the changes seen in osteoporosis. Both micro-MRI and bone biopsies have demonstrated that in osteoporosis, there is a conversion of plates to rods/decreased SC and a disconnection of rods/increased EI (5,18,19). This lower bone quality contributes strongly to decreased bone strength and increased fracture risk in subjects with osteoporosis (6,30). In the Olympic fencers, the apparent trabecular bone microarchitectural adaptations might contribute to the ability of their lower extremities to withstand elevated mechanical loads.

The preliminary results do not demonstrate a difference in trabecular thickness between fencers and controls. The lack of a difference in trabecular thickness in fencers and controls in this study could also be due to the small participant size or inadequate spatial resolution and an inability to detect smaller trabeculae. In prior studies with MR spatial resolution similar to this study (0.156 mm × 0.156 mm, with 1-mm slice thickness), differences in trabecular thickness between patients with age-related osteoporosis and controls were not detectable, and this was attributed to an inability to resolve smaller trabeculae (2– 4,31). Takahashi et al (32) were recently able to detect decreased trabecular thickness in rabbits with glucocorticoid-induced osteoporosis and increased trabecular thickness in risedronate-treated rabbits. Voxel dimensions in this study were 0.097 mm × 0.097 mm with 0.3-mm slice thickness, and this improved spatial resolution could explain their ability to detect changes in trabecular thickness compared to the current study (32). Finally, we cannot exclude the possibility that in response to increased mechanical loads, trabecular bone may adapt, not by increasing trabecular thickness, but by changes in other morphologic and topologic parameters as described above. In future studies, we aim to improve our spatial resolution.

This study has major limitations, including a lack of validation of measurements with another technique and a lack of data regarding the reproducibility of measurements. In a previous study involving nine Olympic fencers, including the four who participated in this

study, qCT scanning of the distal femur demonstrated an approximately 30% to 40% increase (141 mg/mL vs. 104 mg/mL) in distal femoral trabecular bone density compared to matched controls (26). This result correlates with the apparent improvements in trabecular bone microarchitecture demonstrated in this study. However, it should be noted that BMD and trabecular structure can change independently, which is the motivation for using micro-MRI as an additional tool to evaluate osteoporosis (3,4). To validate the measurements, subjects ideally would have been scanned at 1.5T or via microcomputed tomography, but additional scans were declined. In future studies, it will be important to validate the 7T measurements via other imaging techniques or with bone biopsy. Additionally, although studies at low field strength have demonstrated the coefficient of variation of quantitative micro-MR assessments of trabecular bone to be approximately 3% to 8% (33,34), it will be important to obtain this reproducibility data at 7T.

Other limitations of this work include the cross-sectional study design and the small participant size. The cross-sectional study design raises the possibility of selection bias, in which people with inherently better bone structure are more likely to participate in sports because they are better able to endure the physical demands of participation. The authors cannot exclude this possibility, but have tried to match as closely as possible the athletes and controls for age, height, and weight and feel that the main difference between the two groups is the extreme duration and intensity of mechanical loading on the lower extremities. Furthermore, although the participant size is small, apparent differences in trabecular microarchitecture were likely detectable due to a large enough effect size.

In conclusion, this study demonstrates the feasibility of using 7T MRI to produce images of and quantitatively assess trabecular bone microarchitecture in vivo. At 7T, scan times are decreased, and despite increased susceptibility artifact, measurements of trabeculae are similar to those published in prior studies at lower field strength. The results suggest that trabecular bone microarchitecture adapts in response to elevated mechanical stress, lending further support to the concept that trabecular bone structure contributes to bone strength. Future studies are necessary in order to validate measurements made at 7T and to confirm the reproducibility of measurements made at 7T. As imaging techniques are optimized, spatial resolution, SNR, and micro-MR image quality should only improve. Future applications include: the monitoring of osteoporosis and assessment of fracture risk; the investigation of the pathophysiology of other musculoskeletal disorders that involve trabecular bone, such as osteoarthritis; and the imaging of marrow space disorders.

Acknowledgments

We thank the volunteers and members of the 2004 U.S. Olympic Fencing Team for their participation in this study, as well as Kelly Anne McGorty for her assistance with MR scanning. R.R.R. acknowledges support from National Institutes of Health (NIH) grant R01-AR053133-A2.

REFERENCES

1. NIH Consensus Development Panel on osteoporosis prevention, diagnosis, and therapy. Osteoporosis prevention, diagnosis and therapy. JAMA. 2001; 285:785–795. [PubMed: 11176917]
2. Boutry N, Cortet B, Dubois P, Marchandise X, Cotten A. Trabecular bone structure of the calcaneus: preliminary in vivo MR imaging assessment in men with osteoporosis. Radiology. 2003; 227:708–717. [PubMed: 12676974]
3. Link TM, Majumdar S, Augat P, et al. In vivo high resolution MRI of the calcaneus: Differences in trabecular structure in osteoporosis patients. J Bone Miner Res. 1998; 13:1175–1182. [PubMed: 9661082]
4. Majumdar S, Link TM, Augat P, Lin JC, Newitt D, Lane NE, Genant HK. Trabecular bone architecture in the distal radius using magnetic resonance imaging in subjects with fractures of the

proximal femur. Magnetic Resonance Science Center and Osteoporosis and Arthritis Research Group. Osteoporos Int. 1999; 10:231–239. [PubMed: 10525716]

5. Wehrli FW, Gomberg BR, Saha PK, Song HK, Hwang SN, Snyder PJ. Digital topological analysis of in vivo magnetic resonance microimages of trabecular bone reveals structural implications of osteoporosis. J Bone Miner Res. 2001; 16:1520–1531. [PubMed: 11499875]
6. Majumdar S. Magnetic resonance imaging of trabecular bone structure. Top Magn Reson Imaging. 2002; 13:323–334. [PubMed: 12464745]
7. Wehrli FW. Structural and functional assessment of trabecular and cortical bone by micro magnetic resonance imaging. J Magn Reson Imaging. 2007; 25:390–409. [PubMed: 17260403]
8. Saha PK, Gomberg BR, Wehrli FW. Fuzzy distance transform: theory, algorithms and applications. Comput Vis Image Underst. 2002; 86:171–190.
9. Saha PK, Wehrli FW. Measurement of trabecular bone thickness in the limited resolution regime of in vivo MRI by fuzzy distance transform. IEEE Trans Med Imaging. 2004; 23:53–62. [PubMed: 14719687]
10. Saha PK, Chaudhuri BB. 3D digital topology under binary transformation with applications. Comput Vis Image Underst. 1996; 63:418–429.
11. Saha PK, Gomberg BR, Wehrli FW. Three-dimensional digital topological characterization of cancellous bone architecture. Int J Imaging Syst Technol. 2000; 11:81–90.
12. Gomberg BG, Saha PK, Song HK, Hwang SN, Wehrli FW. Application of topological analysis to magnetic resonance images of human trabecular bone. IEEE Trans Med Imaging. 2000; 19:166–174. [PubMed: 10875701]
13. Gold GE, Suh B, Sawyer-Glover A, Beaulieu C. Musculoskeletal MRI at 3.0T: initial clinical experience. AJR Am J Roentgenol. 2004; 183:1479–1486. [PubMed: 15505324]
14. Sell CA, Masi JN, Burghardt A, Newitt D, Link TM, Majumdar S. Quantification of trabecular bone structure using magnetic resonance imaging at 3 Tesla: calibration studies using microcomputed tomography as a standard of reference. Calcif Tissue Int. 2005; 76:355–364. [PubMed: 15868282]
15. Phan CM, Matsuura M, Bauer JS, et al. Trabecular bone structure of the calcaneus: comparison of MR imaging at 3.0 and 1.5 T with micro-CT as the standard of reference. Radiology. 2006; 239:488–496. [PubMed: 16569786]
16. Regatte R, Schweitzer ME. Ultra-high-field MRI of the musculoskeletal system at 7.0 T. J Magn Reson Imaging. 2007; 25:262–269. [PubMed: 17260399]
17. Wolff, J. The law of bone remodeling. Berlin: A. Hirschwald; 1892.
18. Amling M, Posl M, Ritzel H, et al. Architecture and distribution of cancellous bone yield vertebral fracture clues. A histomorphometric analysis of the complete spinal column from 40 autopsy specimens. Arch Orthop Trauma Surg. 1996; 115:262–269. [PubMed: 8836458]
19. Kleerekoper M, Villanueva AR, Stanciu J, Sudhaker Rao D, Parfitt AM. The role of three-dimensional trabecular microstructure in the pathogenesis of vertebral compression fractures. Calcif Tissue Int. 1985; 37:594–597. [PubMed: 3937580]
20. Aaron JE, Francis RM, Peacock M, Makins NB. Contrasting microanatomy of idiopathic and corticosteroid-induced osteoporosis. Clin Orthop Relat Res. 1989:294–305. [PubMed: 2721071]
21. Benito M, Vasilic B, Wehrli FW, et al. Effect of testosterone replacement on trabecular architecture in hypogonadal men. J Bone Miner Res. 2005; 20:1785–1791. [PubMed: 16160736]
22. Chesnut CH, Majumdar S, Newitt DC, et al. Effects of salmon calcitonin on trabecular microarchitecture as determined by magnetic resonance imaging: results from the QUEST study. J Bone Miner Res. 2005; 20:1548–1561. [PubMed: 16059627]
23. Blumenkrantz G, Lindsey CT, Dunn TC, et al. A pilot, two-year longitudinal study of the interrelationship between trabecular bone and articular cartilage in the osteoarthritic knee. Osteoarthritis Cartilage. 2004; 12:997–1005. [PubMed: 15564067]
24. Lindsey CT, Narasimhan A, Adolfo JM, et al. Magnetic resonance evaluation of the interrelationship between articular cartilage and trabecular bone of the osteoarthritic knee. Osteoarthritis Cartilage. 2004; 12:86–96. [PubMed: 14723868]
25. Takahashi M, Uematsu H, Hatabu H. MR imaging at high magnetic fields. Eur J Radiol. 2003; 46:45–52. [PubMed: 12648801]

26. Chang, G.; Regatte, R.; Pakin, KS.; Deoki, R.; Schweitzer, ME. Olympic fencers: changes in cortical vs. trabecular bone determined by qCT. Scientific Abstract number SSG21-04 at the RSNA Scientific Assembly and Annual Meeting; Chicago, IL. 2006.
27. Ward KA, Roberts SA, Adams JE, Mughal MZ. Bone geometry and density in the skeleton of pre-pubertal gymnasts and school children. Bone. 2005; 36:1012–1018. [PubMed: 15876561]
28. Happasalo H, Sievanen H, Kannus P, Heinonen A, Oja P, Vuori I. Dimensions and estimated mechanical characteristics of the humerus after long-term tennis loading. J Bone Miner Res. 1996; 11:864–872. [PubMed: 8725185]
29. Pettersson U, Nordstrom P, Alfredson H, Henriksson-Larsen K, Lorentzon R. Effect of high impact activity on bone mass and size in adolescent females: a comparative study between two different types of sport. Calcif Tissue Int. 2000; 67:207–214. [PubMed: 10954774]
30. Wehrli FW, Song HK, Saha P, Wright AC. Quantitative MRI for the assessment of bone structure and function. NMR Biomed. 2006; 19:731–764. [PubMed: 17075953]
31. Majumdar S, Genant HK, Grampp S, et al. Correlation of trabecular bone structure with age, bone mineral density, and osteoporotic status: in vivo studies in the distal radius using high resolution magnetic resonance imaging. J Bone Miner Res. 1997; 12:111–118. [PubMed: 9240733]
32. Takahashi M, Saha P, Wehrli F. Skeletal effects of short-term exposure of dexamethasone and response to risedronate treatment studied in vivo in rabbits by magnetic resonance micro-imaging and spectroscopy. J Bone Miner Metab. 2006; 24:467–475. [PubMed: 17072739]
33. Gomberg B, Wehrli FW, Vasilic B, et al. Reproducibility and error sources of micro-MRI-based trabecular bone structural parameters of the distal radius and tibia. Bone. 2004; 35:266–276. [PubMed: 15207767]
34. Newitt DC, van Rietbergen B, Majumdar S. Processing and analysis of in vivo high resolution MR images of trabecular bone for longitudinal studies: reproducibility of structural measures and micro-finite element analysis derived mechanical properties. Osteoporos Int. 2002; 13:278–287. [PubMed: 12030542]
35. Wehrli FW, Leonard MB, Saha PK, Gomberg BR. Quantitative high-resolution magnetic resonance imaging reveals structural implications of renal osteodystrophy on trabecular and cortical bone. J Magn Reson Imaging. 2004; 20:83–89. [PubMed: 15221812]

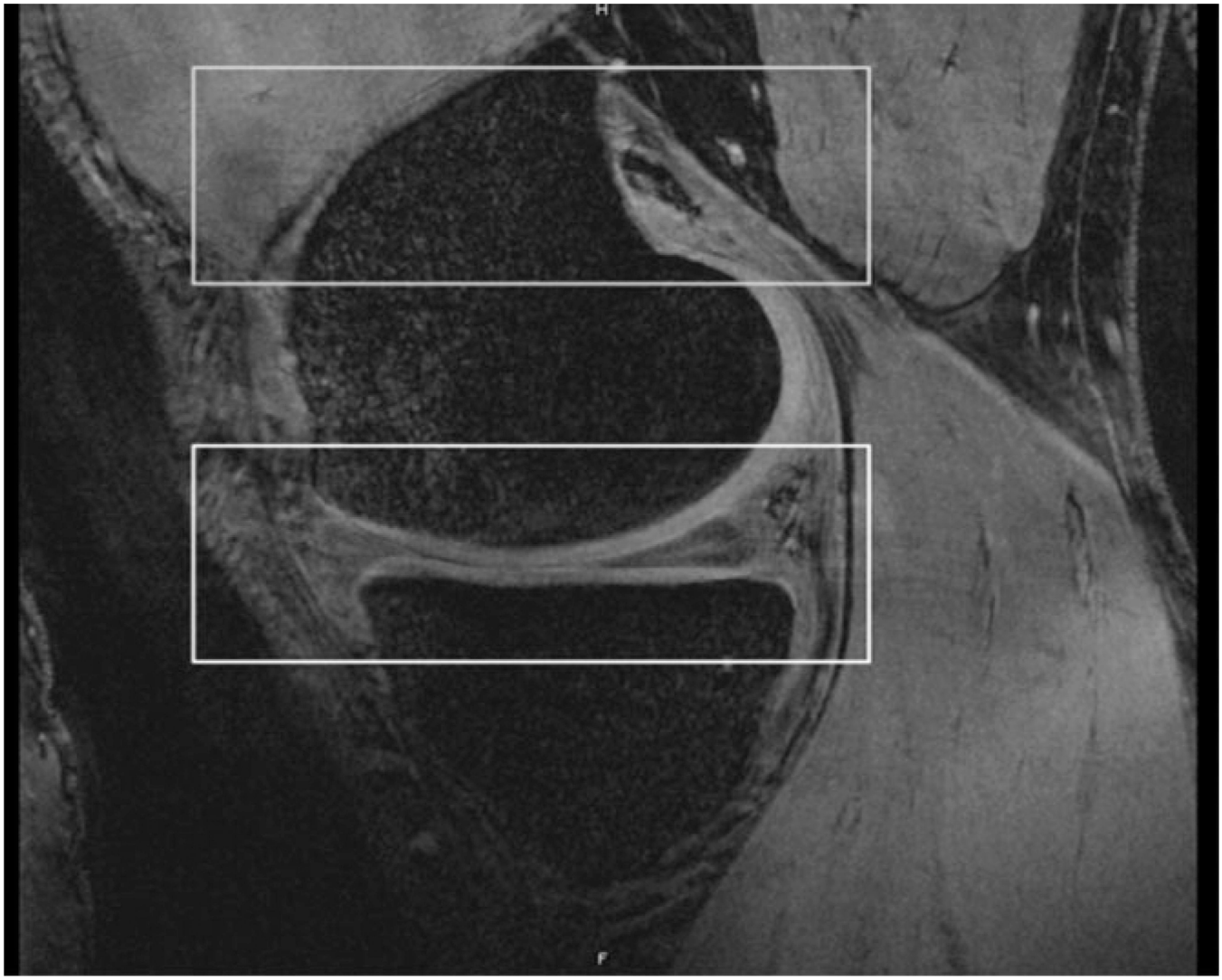

Figure 1.
Sagittal 3D-FLASH 7T MR image of the knee demonstrates the volumes of interest at the distal femur (top box) and knee joint (bottom box) where trabecular bone microarchitecture was quantitatively assessed.

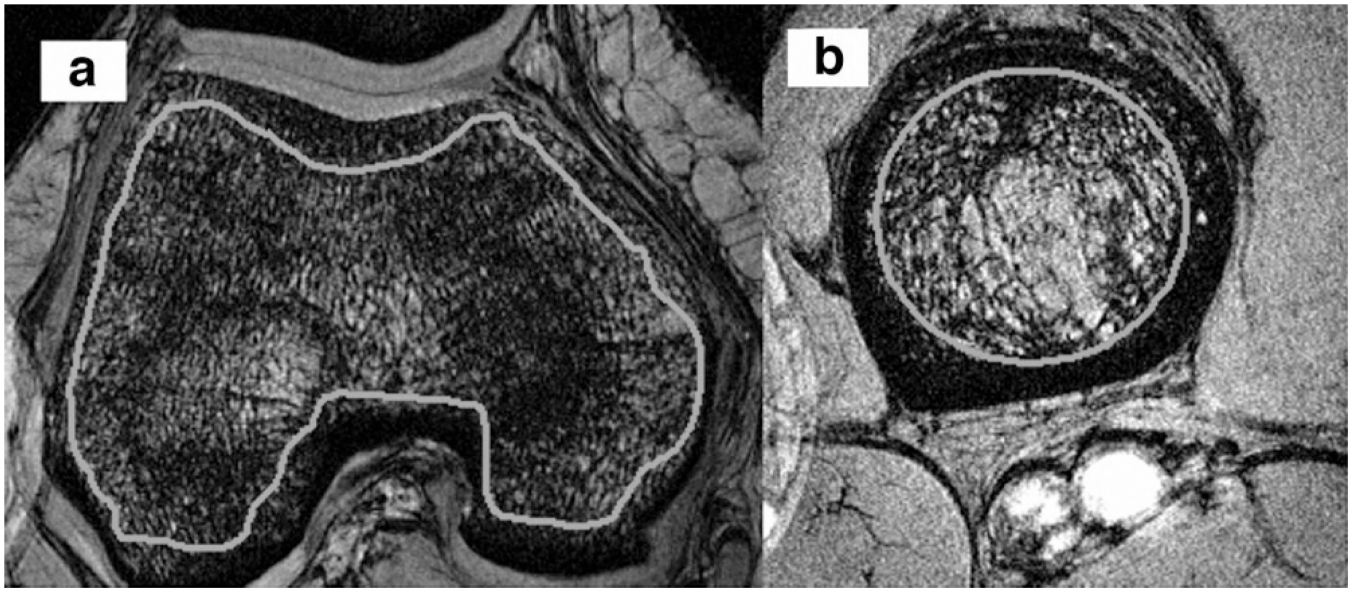

Figure 2.
Representative 3D-FLASH 7T MR axial images of the femoral condyles (**a**) and proximal tibia (**b**) with ROIs placed on trabecular bone.

Table 1

Comparison of Trabecular Bone Morphologic Parameters Between Fencers and Controls at the Distal Femur

Distal femur	Apparent trabecular thickness (mm)	Apparent trabecular separation (mm)	Trabecular number (mm^{-1})	Bone volume fraction
Fencer mean	0.231	0.331	1.24	0.287
Standard deviation	0.0105	0.0140	0.0741	0.00679
Control mean	0.229	0.404	1.06	0.242
Standard deviation	0.00949	0.0196	0.0306	0.00311
P value	$P = 0.71$	$P = 0.0082$	$P = 0.046$	$P = 0.00045$

Table 2

Comparison of Trabecular Bone Morphologic Parameters Between Fencers and Controls at the Knee Joint

Knee joint	Apparent trabecular thickness (mm)	Apparent trabecular separation (mm)	Trabecular number (mm^{-1})	Bone volume fraction
Fencer mean	0.22	0.297	1.35	0.298
Standard deviation	0.00516	0.0027	0.0295	0.00135
Control mean	0.219	0.319	1.28	0.282
Standard deviation	0.00388	0.00988	0.0152	0.00103
P value	$P = 0.92$	$P = 0.051$	$P = 0.0081$	$P = 0.00011$

Table 3

Comparison of Trabecular Bone Topologic Parameters Between Fencers and Controls at the Distal Femur and Knee Joint

Trabecular bone	Surface-curve ratio (femur)	Erosion index (femur)	Surface-curve ratio (joint)	Erosion index (joint)
Fencer mean	8.79	0.852	8.09	0.892
Standard deviation	0.978	0.0275	0.471	0.045
Control mean	5.15	1.35	6.75	1.1
Standard deviation	0.235	0.0458	0.311	0.02
P value	$P = 0.0034$	0.00040	$P = 0.0063$	$P = 0.00084$

Table 4

Comparison of Marrow Space Topologic Parameters Between Fencers and Controls at the Distal Femur and Knee Joint

Marrow space	Surface-curve ratio (femur)	Erosion index (femur)	Surface-curve ratio (joint)	Erosion index (joint)
Fencer mean	27.8	0.29	23.7	0.335
Standard deviation	1.84	0.0216	0.896	0.00675
Control mean	62.6	0.206	32.1	0.286
Standard deviation	5.29	0.00577	1.00	0.00577
P value	$P = 0.0044$	$P = 0.0028$	$P = 0.00028$	$P = 0.00017$

Table 5

Comparison of Quadriceps Muscle Volume Between Fencers and Controls

	Quadriceps muscle volume (mL)
Fencer mean	141
Standard deviation	27.3
Control mean	104
Standard deviation	4.17
P value	$P = 0.038$

Table 6

Comparison of MR Imaging Parameters With the Literature

Study	Body part	Field	Sequence	Imaging time (minutes)	Resolution (mm)	Apparent trabecular thickness (mm)	Bone volume fraction
Link et al., 1998 (3)	Calcaneus	1.5T	3D-GRE	15.15	0.195 × 0.195, 0.5 mm thick	0.600 ± 0.166	0.32 ± 0.07
Majumdar et al., 1999 (4)	Wrist, calcaneus	1.5T	3D-GRE	Not provided	0.156–0.195 × 0.156–0.195, 0.5 mm thick	0.410 ± 0.420	0.28 ± 0.09
Boutry et al., 2003 (2)	Calcaneus	1.5T	3D-GRE	19	0.172 × 0.172, 0.7 mm thick		
Lindsey et al., 2004 (24)	Knee	1.5T	3D-GRE	18.5 (96 images)	0.195 × 0.195, 1 mm thick	0.222 ± 0.006	0.29 ± 0.012
Blumenkrantz et al., 2004 (23)	Knee	1.5T	3D-GRE	18.5	0.195 × 0.195, 1 mm thick		
Wehrli et al., 2004 (35)	Distal tibia	1.5T	3D-spin echo	16.3 (28 images)	0.137 × 0.137, 0.4 mm thick	0.151 ± 0.019	0.12 ± 0.022
Phan et al., 2006 (15)	Calcaneus	1.5T, 3T	3D-GRE	7.5 (64 images)	0.156 × 0.156, 1 mm thick (both 1.5T and 3T)	1.5T: 0.180 ± 0.020; 3T: 0.220 ± 0.020	1.5T: 0.28 ± 0.04; 3T: 0.41 ± 0.04
Current study	Knee	7T	3D-GRE	12 (130 images)	0.156–0.195 × 0.156–0.195, 1 mm thick	0.220 ± 0.005	0.287 ± 0.006

GRE = gradient echo.